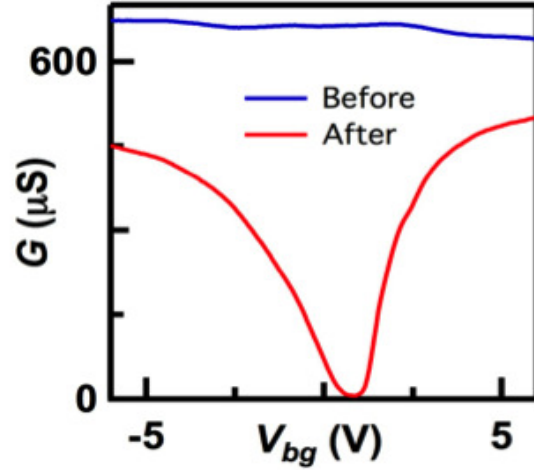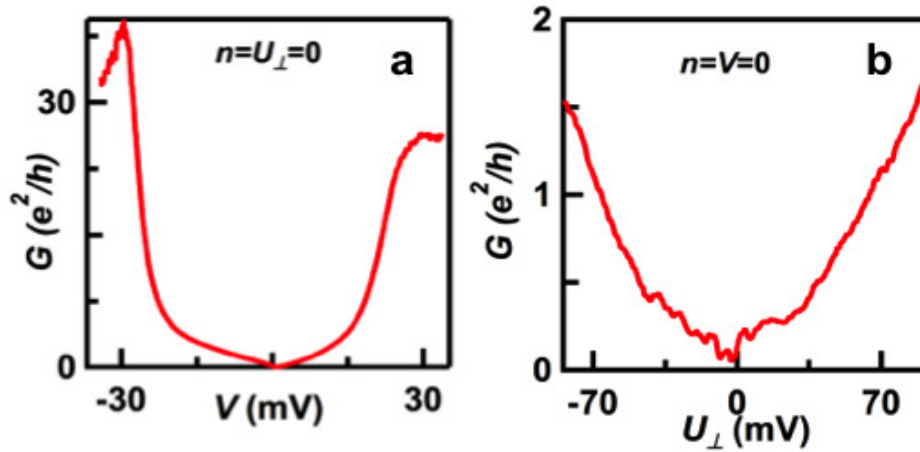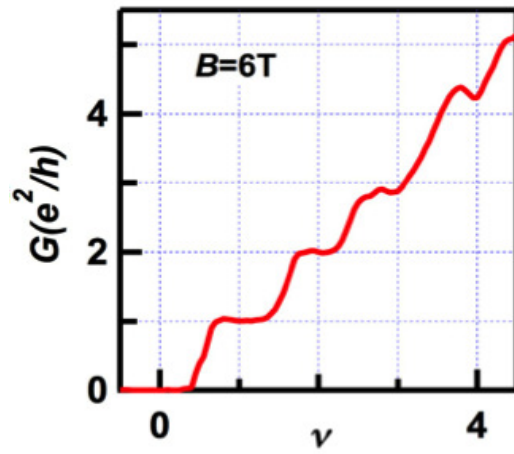# Supplementary Figures

**Supplementary Figure 1**: Device conductance G vs. V_{bg} before and after current annealing.

Supplementary Figure 2: Data from another device at $T = 260$ mK **a.** $G(V)$ at $n = U_\perp = 0$. The sharp peaks indicate $\Delta \sim 30$meV for the device. **b.** $G(U_\perp)$ at $n = V = 0$. Note that the device is insulating state at $U_\perp = 0$, but the conductance exceeds conductance quantum at $|U_\perp| > 70$mV.

Supplementary Figure 3: Conductance vs. filling factor in the quantum Hall regime. The plateaus are well quantized at $\nu = 1$ and 2
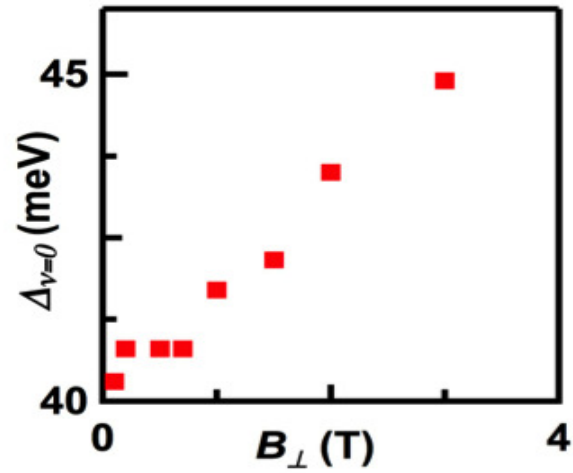
Supplementary Figure 4: Landau level gap for the $\nu = 0$ state vs. $B_\perp$

Supplementary note 1 : Hartree model of screening in ABC-stacked trilayer graphene

We self-consistently calculate screening of ABC-stacked TLG using a procedure similar to that for bilayer graphene [1].In the presence of voltages applied to the gates, from Gauss' Law, we have

$$n = n_1 + n_3 = \frac{\epsilon_0 \epsilon_b V_b}{e h_b} + \frac{\epsilon_0 \epsilon_t V_t}{e h_t}, \tag{1}$$

$$U_\perp^s = -\frac{\epsilon_t V_t d e}{\epsilon_r h_t} + \frac{d e^2 n_3}{\epsilon_0 \epsilon_r}. \tag{2}$$

In these equations, e the electron charge, ϵ the dielectric constant, V the voltage applied to the gate, ϵ_0 the permittivity of vacuum, $d = 0.67$ nm is the distance between the outmost layers, h the distance between graphene and the gate, n_1 and n_3 are the charge densities on the bottom and top layers of the trilayer, and ϵ_r is the dielectric constant of the trilayer itself. The subscripts b and t indicate the back gate and top gate, respectively. $U_\perp^s$ is the potential across the trilayer that is to be determined. Now the externally imposed interlayer potential is given by,

$$U_\perp = \left(\frac{\epsilon_b V_b}{h_b} - \frac{\epsilon_r V_t}{h_t} \right) \frac{e d}{2}. \tag{3}$$

which gives

$$U_\perp^s = U_\perp + \frac{d e^2}{2 \epsilon_0 \epsilon_r} (n_3 - n_1). \tag{4}$$

In r-TLG, inequivalent sublattices A_i and B_i are arranged in following sequence: one of the two-carbon atom sites in both the top and bottom layer $B_1(A_3)$ has a different near-neighbor carbon atom site in the middle layer $A_2(B_2)$, which leaves one-carbon atom site in the top and bottom layers $A_1(B_3)$ without a near-neighbor in the middle layer. Interlayer hopping on adjacent layer near-neighbor carbon atom sites leads to the formation of high-energy dimer bands, which push the electron energy away form the Fermi surface, leaving one low-energy sublattice site per π -carbon orbital in the outermost layers. The effective two-band Hamiltonian for r-TLG [2]

$$\begin{pmatrix} -\frac{U_\perp^s}{2} & \frac{v^3}{\gamma_1^2}(p_x - i p_y)^3 \\ \frac{v^3}{\gamma_1^2}(p_x + i p_y)^3 & \frac{U_\perp^s}{2} \end{pmatrix}, \tag{5}$$

operates on the pseudospinor $\psi_K^\dagger = (\psi_{A_1,K}^\dagger, \psi_{B_3,K}^\dagger)$, where the $\psi_{i,K}^\dagger$ is the envelop wavefunction of sublattice i at valley K, with the pseudospinor in valley K' $\psi_{K'}^\dagger = \hat{\tau}^x \psi_K^\dagger$, $\hat{\tau}^x$ is the Pauli matrix in pseudospin space. The eigenvalues and wave functions are

$$E = \pm \sqrt{\frac{(U_\perp^s)^2}{4} + \frac{v^6 |p|^6}{\gamma_1^4}} \qquad \psi = \begin{pmatrix} \psi_{A_1} \\ \psi_{B_3} \end{pmatrix} = \sqrt{\frac{E - U_\perp^s/2}{2E}} \begin{pmatrix} 1 \\ -\frac{v^3 |p|^3}{\gamma_1^2} \frac{1}{(E - U_\perp^s/2)} e^{3i\varphi} \end{pmatrix} e^{i\mathbf{p}\cdot\mathbf{r}/\hbar}, \tag{6}$$

here v is the Fermi velocity of monolayer graphene, p is the momentum, $\gamma_1 \sim 0.4$ eV is the nearest neighbour interlayer hopping energy, $\varphi = \tan^{-1}(p_y/p_x)$, and $\hbar = h/2\pi$ where h is Planck's constant. The layer densities can be calculated from

$$n_1 = \frac{2}{\pi \hbar^2} \int |\psi_{A_1}|^2 p dp \qquad n_2 = \frac{2}{\pi \hbar^2} \int |\psi_{B_3}|^2 p dp \tag{7}$$

For the hole-doped regime, the Fermi level is in the valence band, so

$$n_1 = \frac{2}{\pi \hbar^2} \int_{p_F}^\infty \left(\frac{E - U_\perp^s/2}{2E} \right) p dp = \frac{n}{2} + \frac{2}{\pi \hbar^2} \frac{U_\perp^s}{4} \int_{p_F}^\infty \frac{p dp}{\frac{U_\perp^s}{2} \sqrt{1 + \frac{4 v^6 |p|^6}{\gamma_1^4 (U_\perp^s)^2}}}. \tag{8}$$

Defining $x_F = (4/((U_\perp^s)^2 \gamma_1^4))^{1/3} v^2 \pi \hbar^2 n$, we can express n_1 as

$$n_1 = \frac{n}{2} + \frac{1}{2\pi \hbar^2} \left(\frac{(U_\perp^s)^2 \gamma_1^4}{4 v^6} \right)^{1/3} \int_{x_F}^\infty \frac{dx}{\sqrt{1 + x^3}} = \frac{n}{2} + \frac{1}{2\pi \hbar^2} \left(\frac{(U_\perp^s)^2 \gamma_1^4}{4 v^6} \right)^{1/3} \left(2.8 - \int_0^{x_F} \frac{dx}{\sqrt{1 + x^3}} \right). \tag{9}$$

Similarly,

$$n_3 = \frac{n}{2} - \frac{1}{2\pi\hbar^2}\left(\frac{(U_\perp^s)^2\gamma_1^4}{4v^6}\right)^{1/3}\left(2.8 - \int_0^{x_F}\frac{dx}{\sqrt{1+x^3}}\right) \tag{10}$$

So that

$$n_3 - n_1 = \frac{1}{\pi}\left(\frac{\gamma_1}{\hbar v}\right)^2\left(\frac{U_\perp^s}{2\gamma_1}\right)^{2/3}\left[\int_0^{x_F}\frac{dx}{\sqrt{1+x^3}} - 2.8\right]. \tag{11}$$

Substituting into Eq. 4, we obtain,

$$U_\perp^s = U_\perp + \frac{de^2}{2\epsilon_0\epsilon_r}\frac{1}{\pi}\left(\frac{\gamma_1}{\hbar v}\right)^2\left(\frac{U_\perp^s}{2\gamma_1}\right)^{2/3}\left[\int_0^{x_F}\frac{dx}{\sqrt{1+x^3}} - 2.8\right]. \tag{12}$$

that can be solved numerically for $U_\perp^s$ for given $U_\perp$ and n (the dependence on n comes through x_F). Note that screening is more effective for smaller n, due to the larger density of states near the charge neutrality point.

Supplementary note 2 : Data from another device at $B = 0$

We have observed the intrinsic insulating state at $n = U_\perp = 0$ in 5 different r-TLG devices, with a gap ranging from $20 - 40$ meV that can be suppressed by $U_\perp$ of either polarity. Supplementary Fig.2 displays data from another device at the charge neutrality point. The $G(V)$ curve displays a flat, insulating region around zero source drain bias, and sharp peaks at ± 30mV, indicating $\Delta \sim 30$ meV for this device. This insulating state is completely suppressed upon application of $|U_\perp|$ the zero bias conductance increases to $\sim 1.5e^2/h$ at $|U_\perp| = 70$ mV, indicating that this interaction-induced gap can be closed by interplayer asymmetry of either polarity.

Supplementary note 3 : Screening length in an ABC trilayer

The interplay between band structure effects and interactions in an ABC trilayer allows us to define at least four important length scales: i) The scale associated to the momentum beyond which the effects of the main interlayer hopping term, γ_1, are small, and the bands resemble those of three independent graphene layers, $\ell_\perp \approx v_F/\gamma_1$, where $v_F = 3\gamma_0 a/2$, and $a \approx 1.4$ Å is the distance between neighboring carbon atoms in a given plane, ii) The inverse of the momentum at which the band structure changes smoothly from a cubic to a quadratic dispersion, ℓ_{BS}, iii) The Fermi-Thomas screening length, ℓ_{FT}. This length goes to zero at the edge of a band which a cubic dispersion on momentum, so that it should be estimated at the crossover momentum $k \approx \ell_{BS}^{-1}$. Finally, iv) the ABC trilayer has a finite with, $d \approx 2 \times d_{BLG}$, where d_{BLG} is the interlayer distance in bilayer graphene.

We assume in the following that $\gamma_4 \ll \gamma_3 \approx \gamma_1 \ll \gamma_0$. The value of $\ell_\perp$ is

$$\ell_\perp \approx a\frac{3\gamma_0}{2\gamma_1} \tag{13}$$

The bands at low energies are

$$\epsilon_k \approx \pm\frac{3}{2}\left|\frac{9\gamma_0^3}{4\gamma_1^2}(ka)^3e^{3i\phi_k} + \frac{3\gamma_0\gamma_3}{2\gamma_1}(ka)^2\right| \tag{14}$$

where $\phi_k = \arctan(k_y/k_x)$. Using this expression, we obtain

$$\ell_{BS} \approx a\frac{3\gamma_0^2}{4\gamma_1\gamma_3} \tag{15}$$

The Fermi Thomas wavelength is

$$k_{FT} \approx \frac{8e^2\gamma_1^2}{81\epsilon_0\gamma_0^3 k_{BS}} \tag{16}$$

where ϵ_0 is the dielectric constant, and $k_{BS} = \ell_{BS}^{-1}$. Using eq.15, we find

$$\ell_{FT} \approx a\frac{9\gamma_3}{\alpha\gamma_1} \tag{17}$$

where $\alpha = e^2/(\epsilon_0 v_F)$ is the fine structure constant of graphene.

We take $\gamma_0 = 2.7$ eV, $\gamma_1 = 0.4$ eV, and $\gamma_3 = 0.3$ eV. In order to estimate the screening length, we assume that in a suspended sample, $\epsilon_0 = 1$, and $\alpha \sim 2.4$. We finally take $d_{BLG} \approx 0.34$ nm. Then, the previous analysis leads to

$$\ell_{\perp} \approx 1.4\text{nm}$$
$$\ell_{BS} \approx 6.4\text{nm}$$
$$\ell_{FT} \approx 0.4\text{nm}$$
$$d \approx 0.7\text{nm} \tag{18}$$

This analysis gives $\ell_{FT} \lesssim d$. This overestimates screening in the perpendicular direction, as the electronic states which give rise to the screening cloud are given by a coherent superposition of waves localized in the top and bottom layers. This state cannot be polarized in the direction normal to the layers. Screening in the perpendicular direction should be such that $\ell_{FT} \approx d$.

Supplementary note 4 : Estimation of the Antiferromagnetic Gap

The cubic dispersion of r-TLG's bands at low energies leads to a density of states that diverges as $D(\epsilon) \propto \epsilon^{-1/3}$ at low energies. Local interactions give rise to perturbations which should lead to a broken symmetry phase at low temperatures. The divergence encountered when studying interaction effects within perturbation theory is more severe than the logarithmic divergence found in graphene bilayers. We expect the broken symmetry phase to be more stable in a graphene trilayer than in a graphene bilayer. The renormalization group methods that can be applied in a bilayer [5, 6, 12] do not work for a trilayer, but, on the other hand, we expect that a mean field analysis should be more reliable, as the low temperature phase is more robust.

A classification of possible gapped phases in an ABC trilayer has been discussed in [13], and a calculation of relative energies can be found in [14]. For a bilayer with short range interactions the most likely phase is either a layer antiferromagnet or a nematic phase [16, 17]. In particular, an on site Hubbard interaction leads to a layer antiferromagnet [18]. We present here a simple analysis of a gapped layered antiferromagnetic phase (note that a nematic phase is gapless) using mean field theory, see also [14]. The magnitude of the local interactions in graphene and graphite is not determined, but different estimates suggest that the Hubbard onsite interaction is $U \approx 5-10$eV [19, 21]. We use an effective Hamiltonian reduced to two sites, one in the top and the other in the bottom layer (see Eq. 5) and a local Hubbard interaction

$$H_{int} = U \sum_i \left(n_{i\uparrow} - \frac{1}{2} \right)\left(n_{i\downarrow} - \frac{1}{2} \right) \tag{19}$$

where the label i runs over all sites in the reduced hamiltonian. We assume that an antiferromagnetic gap, Δ, emerges at low temperatures. The mean field equations give

$$\Delta = U \left(\langle n_\uparrow \rangle - \langle n_\downarrow \rangle \right)$$
$$1 = \frac{U\Omega}{2\pi} \int_0^\infty \frac{kdk}{\sqrt{\left(\frac{\hbar^3 v_F^3 k^3}{\gamma_1^2}\right)^2 + \frac{\Delta^2}{4}}} \tag{20}$$

where $\Omega = (3\sqrt{3}a^2)/2$ is the area of the unit cell. Thus we find

$$\Delta \approx 2 \times \left(\frac{cU\Omega}{2\pi\hbar^2 v_F^2} \right)^3 \gamma_1^4 = 2 \times \left(\frac{c}{\pi\sqrt{3}} \right)^3 \frac{\gamma_1^4 U^3}{\gamma_0^6} \tag{21}$$

where $c = \int_0^\infty dx/\sqrt{1+x^3} = [2\Gamma(1/3)\Gamma(7/6)]/\sqrt{\pi} \approx 2.8$. We note that U has only been theoretically estimated, but never experimentally measured for graphene. For $\gamma_0 \approx 2.7$eV, $\gamma_1 \approx 0.4$eV, and $U \approx 10$ eV, the antiferromagnetic gap $\Delta \approx 18$ meV. This value is lower than the experimental result.

The previous analysis, however, neglects the long range part of the interaction. In single layer and in multilayered graphene, exchange processes associated to the $q \to 0$ part of the interaction can enhance preexisting gaps, or even trigger their existence[22, 23]. Screening in an ABC trilayer is determined by the polarizability[24]

$$\chi(\vec{q}) = N \sum_{\vec{k}} \left[\frac{1 - \cos\left(3\theta_{\vec{k}+\vec{q}/2, \vec{k}-\vec{q}/2}\right)}{2} \right] \frac{1}{\hbar^3 v_F^3 / \gamma_1^2 \left(\left|\vec{k}+\vec{q}/2\right|^3 + \left|\vec{k}+\vec{q}/2\right|^3 \right)} = \frac{c_\chi \gamma_1^2}{\hbar^3 v_F^3 |\vec{q}|} \tag{22}$$

where $c_\chi \approx 0.24$, $N = 4$, and $\theta_{\vec{k}+\vec{q}/2, \vec{k}-\vec{q}/2}$ is the angle between vectors $\vec{k}+\vec{q}/2$ and $\vec{k}-\vec{q}/2$. Using the RPA, the effective interaction becomes $v_{\vec{q}} \approx \chi^{-1}(\vec{q})$. The correction to the gap can be written as

$$\delta\Delta(\vec{q}) \approx \sum_{\vec{q}'} v_{\vec{q}-\vec{q}'} \frac{\Delta_0(\vec{q}')}{(\hbar^3 v_F^3 \vec{q}'^3)/\gamma_1^2} \tag{23}$$

We make the ansatz that Δ_0 is independent of $\vec{q}$. Then, we obtain the approximate scaling equation

$$\frac{\Lambda}{\Delta} \frac{\partial \Delta}{\partial \Lambda} \approx \frac{1}{2\pi c_\chi} \tag{24}$$

where Λ is a high momentum cutoff. This equation leads to the new, Δ, including self consistently the exchange effects

$$\Delta_{ex} \approx \Delta \left(\frac{\gamma_1}{\Delta}\right)^{\frac{\alpha}{1+\alpha}} \tag{25}$$

where $\alpha \approx 1/(6\pi c_\chi)$, and we assume that the high momentum cutoff is such that $(\hbar^3 v_F^3 \Lambda^3)/\gamma_1^2 \approx \gamma_1$. This analysis leads to an enhancement of the gap by about a factor of two.

Finally, the total spin per carbon atom in a given layer is

$$s = \pm\frac{\Delta}{U} \times \mu_B \tag{26}$$

where μ_B is Bohr's magneton. For the gap estimated in eq.(20) we find $s \approx \pm 10^{-3} \mu_B$.

Supplementary References

[1] E. McCann, M. Koshino, The electronic properties of bilayer graphene. *Rep. Prog. Phys.* **76**, 056503 (2013).

[2] Fan Zhang, Bhagawan Sahu, Hongki Min, and A. H. MacDonald, Band structure of -stacked graphene trilayers. *Phys. Rev. B* **82**, 035409 (2010).

[3] Y. Barlas, K. Yang and A. H. MacDonald, Quantum Hall effects in graphene-based two-dimensional electron systems. *Nanotechnology* **23**, 052001 (2012)

[4] H. J. v. Elferen et al., preprint, Fine structure of the lowest Landau level in suspended trilayer graphene. *Phys. Rev. B* **88**, 121302(R) (2013).

[5] J. Nilsson, A. H. Castro Neto, N. M. R. Peres, and F. Guinea, Electron-electron interactions and the phase diagram of a graphene bilayer. *Phys. Rev. B* **73**, 214418 (2006).

[6] E. McCann, D. L. Abergel, and V. I. Falko, Electrons in bilayer graphene *Solid St. Commun.* **143**, 110 (2007).

[7] O. Vafek and K. Yang, Many-body instability of Coulomb interacting bilayer graphene: Renormalization group approach. *Phys. Rev. B* **81**, 041401 (2010).

[8] R. Nandkishore and L. Levitov, Quantum anomalous Hall state in bilayer graphene. *Phys. Rev. B* **82**, 115124 (2010)

[9] F. Zhang, H. Min, M. Polini, and A. H. MacDonald, Spontaneous inversion symmetry breaking in graphene bilayers. *Phys. Rev. B* **81**, 041402 (2010).

[10] Y. Barlas and K. Yang, Non-Fermi Liquid behavior in Neutral Bilayer Graphene. *Phys. Rev. B* **80**, 161408(R) (2009).

[11] R. Nandkishore and L. Levitov, Electron interactions in bilayer graphene: Marginal Fermi liquid and zero-bias anomaly *Phys. Rev. B* **82**, 115431 (2010).

[12] Y. Lemonik, I. L. Aleiner, C. Toke, and V. I. Fal'ko, Spontaneous symmetry breaking and Lifshitz transition in bilayer graphene. *Phys. Rev. B* **82**, 201408 (2010).

[13] F. Zhang, J. Jung, G. A. Fiete, Q. Niu, and A. H. MacDonald, Spontaneous Quantum Hall States in Chirally Stacked Few-Layer Graphene Systems. *Phys. Rev. Lett.* **106**, 156801 (2011).

[14] Jeil Jung and Allan H. MacDonald, Gapped broken symmetry states in ABC-stacked trilayer graphene *Phys. Rev. B* **88**, 075408 (2013).

[15] O. Vafek, Interacting fermions on the honeycomb bilayer: From weak to strong coupling. *Phys. Rev. B* **82**, 205106 (2010).

[16] R. E. Throckmorton and O. Vafek, Fermions on bilayer graphene: symmetry breaking for B=0 and $\nu = 0$, *Phys. Rev. B* **86**, 115447 (2012) arXiv:1111.2076.

[17] Y. Lemonik, I. L. Aleiner, and V. I. Fal'ko, Competing nematic, antiferromagnetic, and spin-flux orders in the ground state of bilayer graphene. *Phys. Rev. B* **85**, 245451 (2012).

[18] T. C. Lang, Z. Y. Meng, M. M. Scherer, S. Uebelacker, F. F. Assaad, A. Muramatsu, and C. Honerkamp, Antiferromagnetism in the Hubbard Model on the Bernal-Stacked Honeycomb Bilayer *Phys. Rev. Lett.* **109**, 126402 (2012).

[19] J. A. Vergés, E. San Fabián, G. Chiappe, and E. Louis, Fit of Pariser-Parr-Pople and Hubbard model Hamiltonians to charge and spin states of polycyclic aromatic hydrocarbons. *Phys. Rev. B* **81**, 085120 (2010).

[20] T. O. Wehling, *et. al.*, Strength of Effective Coulomb Interactions in Graphene and Graphite. *Phys. Rev. Lett.* **106**, 236805 (2011).

[21] M. Schüler *et. al.*, Optimal Hubbard Models for Materials with Nonlocal Coulomb Interactions: Graphene, Silicene, and Benzene. *Phys. Rev. Lett.* **111**, 036601 (2013).

[22] D. V. Khveshchenko, Ghost Excitonic Insulator Transition in Layered Graphite. *Phys. Rev. Lett.* **87**, 246802 (2001).

[23] E. V. Gorbar, V. P. Gusynin, V. A. Miransky and I. A. Shovkovy, Magnetic field driven metal-insulator phase transition in planar systems. *Phys. Rev. B* **66**, 045108 (2002).

[24] Ralph van Gelderen, Richard Olsen, and C. Morais Smith, Screening in multilayer graphene. *Phys. Rev. B*, **88**, 115414 (2013).